Asian Journal of Atmospheric Environment
Vol. 10-3, pp. 125-136, September 2016
doi: http://dx.doi.org/10.5572/ajae.2016.10.3.125

ISSN (Online) 2287-1160
ISSN (Print) 1976-6912

Mitigation of Ammonia Dispersion with Mesh Barrier under Various Atmospheric Stability Conditions

M. Barzegar Gerdroodbary*, Mojtaba Mokhtari[1)], Shervin Bishehsari[2)] and Keivan Fallah[3)]

Department of Mechanical Engineering, Babol University of Technology, Babol, Iran
[1)]Department of Chemical and Petroleum Engineering, Sharif University of Technology, Tehran, Iran
[2)]Department of Mechanical Engineering, Central Tehran Branch, Islamic Azad University, Tehran, Iran
[3)]Department of Mechanical Engineering, Sari Branch, Islamic Azad University, Sari, Iran

*Corresponding author. Tel: +98-11-32334205, E-mail: mbarzegarg@yahoo.com

ABSTRACT

In this study, the effects of the mesh barrier on the free dispersion of ammonia were numerically investigated under different atmospheric conditions. This study presents the detail and flow feature of the dispersion of ammonia through the mesh barrier on various free stream conditions to decline and limit the toxic danger of the ammonia. It is assumed that the dispersion of the ammonia occurred through the leakage in the pipeline. Parametric studies were conducted on the performance of the mesh barrier by using the Reynolds-averaged Navier-Stokes equations with realizable k-ε turbulence model. Numerical simulations of ammonia dispersion in the presence of mesh barrier revealed significant results in a fully turbulent free stream condition. The results clearly show that the flow behavior was found to be a direct result of mesh size and ammonia dispersion is highly influenced by these changes in flow patterns in downstream. In fact, the flow regime becomes laminar as flow passes through mesh barrier. According to the results, the mesh barrier decreased the maximum concentration of the ammonia gas and limited the risk zone (more than 500 ppm) lower than 2 m height. Furthermore, a significant reduction occurs in the slope of the upper boundary of NH_3 risk zone distribution at downstream when a mesh barrier is presented. Thus, this device highly restricts the leak distribution of ammonia in the industrial plan.

Key words: Atmospheric dispersion, Mesh barrier, Ammonia, Numerical simulation, Accidental release

1. INTRODUCTION

Several researches (Galeev, 2013a; Labovský *et al.*, 2011) have shown that people who live and work near petrochemical plant and/or gas storages area are at risk for a variety of health problems such as respiratory and cardiovascular problems and danger of death due to exposure to harmful leaking pollutants of hazardous gases such as CO and NH_3. Recently, various scientists (Galeev, 2013b; Mack *et al.*, 2013; Pandya *et al.*, 2012) have focused on free dispersion of toxic gas as a main concern of different industrial plants. Since ammonia is a common substance, which has many uses owing to its chemical and physical properties, it is widely used in various applications (refrigerators, condensors). Furthermore, ammonia is a substance that is extremely toxic, explosive, flammable and corrosive in certain conditions. The accidental loss of this gas definitely leads a disaster which may be unpredictable. It cannot be forgotten that the failure of a storage tank of ammonia in Dakar on March 24, 1992, caused a large number of fatalities (129 dead and more than 1100 injured) some of which were due to the toxic nature of ammonia and occurred several weeks after the accident.

An extensive research effort has been developed worldwide on the prediction and mitigation of accidental loss of toxic gas (Vallero *et al.*, 2015; Cheng *et al.*, 2014; Jeong, 2014; Ng and Chau, 2014; Galeev, 2014, 2013b; Khan *et al.*, 2000). Cheng *et al.* (2014) used water curtain system to mitigate ammonia vapor cloud. Jeong (2014) investigated the effect of a double barrier on the dispersion of CO in the downstream. Nonetheless, few solutions have been proposed for conventional dispersion caused by leakage. Mesh barriers, which are studied here, are a novel device that reduce vortices in the downstream, and this increases the concentration of the ammonia on the ground surface. Our goal is to investigate the efficiency of such a device in various atmospheric conditions. We have found that this device has, in fact, the advantage of being an economical method to reduce the danger of dispersion of toxic and flammable gases. Moreover, this device will be particularly attractive, because it can be easily installed in industrial plants; additionally,

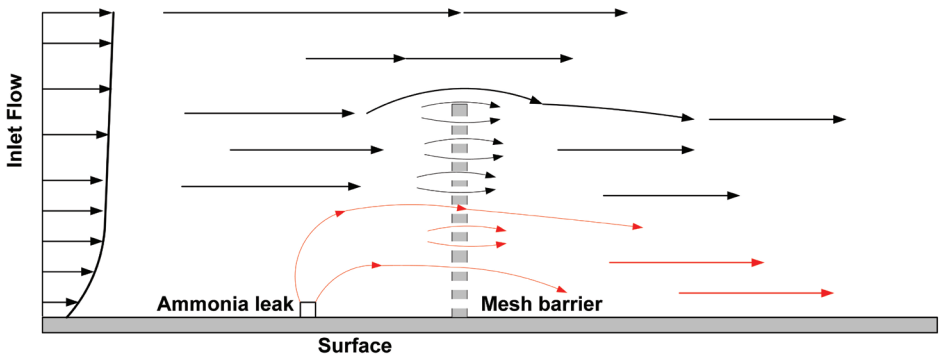

Fig. 1. Schematic representation of the flow features around mesh barrier.

it is expected to direct leak to the ground in downstream and thereby help in the detection of leak and prevent more loss.

A large number of studies have been available in the field of the dispersion of air pollution over the last 30 years (Bubbico *et al*., 2014; Schulte *et al*., 2014; Sklavounos *et al*., 2014; Steffens *et al*., 2013, 2012; Dandrieux *et al*., 2001; Khan *et al*., 1999a, b). Most of these researches are focused on the behavior and quantification of spatial and temporal concentration profiles of pollutant resulting from loss of toxic and/or dangerous substances such as CO and CO_2. Furthermore, studies in this area typically investigate methods to improve the distribution of pollution in urban areas to reduce high concentration regions, which are most often termed "air pollution".

The correct prediction of concentration profiles can not only help in designing mitigation/prevention equipment such as gas detection alarms and shutdown procedures, but also help decide on modifications that may help prevent any escalation of the event. Although several investigations revealed detailed understanding of the near field dispersion of various toxic gases, there have been few studies on prevention and limitation of this phenomenon.

A schematic diagram of freestream leakage from a pipe in the presence of a mesh barrier is shown in Fig. 1. In the flow field, the ammonia released from the pipeline, and the free stream air winds are from upstream. As ammonia and air move to the downstream side for a short distance, the micro holes affect the structure of the stream and it becomes uniform.

The main scope of the present study is to investigate the effects of a mesh barrier on the distribution of ammonia gas. Also, various leak conditions (mass flow rate and jet direction) and the mesh space of the barrier are studied to reveal the effects of each on dispersion of ammonia leak in downstream of the flow. Moreover, this work reveals the influence of the distance of the barrier from a leak on the distribution of ammonia gas downstream for various atmospheric conditions.

The flow structure is numerically simulated by solving the Reynolds-Averaged Navier-Stokes equations. The numerical solution is first validated with experimental data for free dispersion of ammonia. Then, parametric study is conducted to investigate the performance of the barrier on dispersion.

2. NUMERICAL APPROACH

2.1 Geometry and Grid

This investigation focuses on the injection of an ammonia leak from the pipeline a cross to the free stream flow on a flat surface. The main size of model is obtained from Bouet *et al*. (2005). The computational domain selected for the present simulation is a surface 100 m-long and 30 m-high along the center of the leakage, and employs two dimensional in order to reduce computational expense. Fig. 2a illustrates the size of the main model of the domain and the barrier. The same geometry without the mesh barrier was also used to compare and evaluate the performance of this device.

A mesh barrier was used to control the dispersion of the ammonia leak. Various mesh sizes have been investigated to define the optimum size for mitigation of the dispersion. The height of the barrier was assumed to be 5 m.

In order to quantify the characteristic of each barrier configuration, it is necessary to define a proper non-dimensional number known as the Mesh Coefficient (MC). The required relation is given as

$$Mesh\ Coefficient\ (MC) = N \times \frac{\sum S}{L} \quad (1)$$

Where $\sum S$ is the sum of the areas of each block

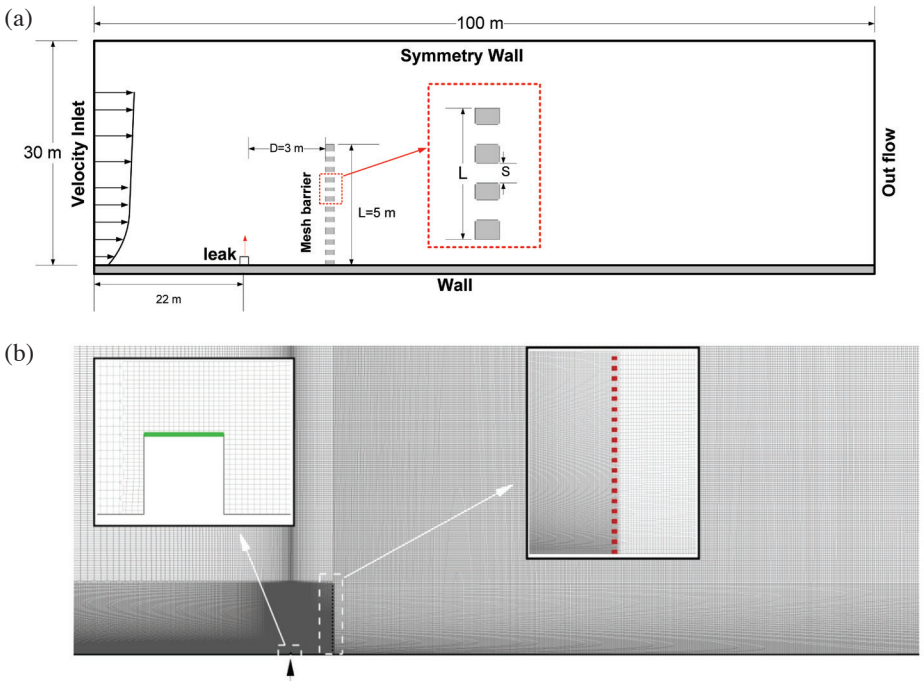

Fig. 2. (a) Computational of domain and (b) grid generation of the main model.

space, N is the number of the hole in the barrier and L is the total length of the block of the barrier. In the present study, eight types of mesh barrier, with various Mesh Coefficients (MC), have been investigated for different atmospheric conditions. Furthermore, the distance of the mesh barrier for main model is 3 m.

In 1961, Pasquill (1961) presented most commonly used method of categorizing the amount of atmospheric turbulence. He categorized the atmospheric turbulence into six stability classes named A, B, C, D, E and F with class A being the most unstable or most turbulent class, and class F the most stable or least turbulent class. In order to cover all aspects of the this method, three main atmospheric conditions (A, D, F) are chosen for this works.

In the present model, the main interactions occur close to the barrier and completely within the boundary layer. Since fine meshes were required to adequately resolve the flow features, the domain was broken down into separate computational units to work within the constraints of available computational resources, as shown in Fig. 2b.

Full structured grids were constructed for all cases. One of the main factors of the analyzing the grid is Y^+. Y^+ is a non-dimensional distance that is often used to describe how coarse or fine a mesh is for a particular flow pattern. It is important in turbulence modeling to determine the proper size of the cells near domain walls. The turbulence model wall laws have restrictions on the y^+ value at the wall. In our study, cell refinement was achieved manually in the region immediately adjacent to each outlet of leak and, in the wall normal direction, the cells were arranged such that the distance from the wall to the first cell centroid provided a Y^+ within the acceptable range ($Y^+ < 30$) of turbulence model. The grid spacing was stretched ensure all regions of the boundary layer and injection flow structures close to the wall were adequately resolved. An example of the grid in the vicinity of an injector is shown in Fig. 2b together with a close-up view of the grid in the vicinity of the leakage and mesh barrier are displayed in the Fig. 2b.

One of the main factors for the numerical simulation is a proper grid arrangement. The structural grid is generated to improve the accuracy of results. Also, an extensive grid refinement study (mesh sizes from 860×260, 1100×340 and 1400×420 in the horizontal and vertical directions) was conducted to determine grid independence in mass distribution to resolve the boundary layers. The results of validation (Fig. 3) show that a fine grid (300000) has enough precision for the present investigation.

2.2 Freestream and Boundary Condition

The types of boundary conditions are defined as depicted in Fig. 2a. The conditions that apply to the

inflow boundary are a velocity inlet, where profiles of wind speed, turbulent dissipation and TKE must be provided. The outlet is set to be a simple outflow condition. The top of the domain, assumed to be sufficiently far away from the mesh barrier as to not affect the flow in the area, is set to a symmetry condition.

The inlet condition of the domain needs careful attention as inlet flow conditions will greatly influence on the simulation results. The standard power law atmospheric boundary layer profile, turbulence kinetic energy (k) and dissipation (ε) at the inlet boundaries are given by equation (2).

$$U_{(z)} = U_*\left(\frac{Z}{Z_*}\right)^P,\ k = \frac{U_*^2}{\sqrt{c_\mu}},\ \varepsilon = \frac{U_*^3}{k_v(Z+Z_*)} \tag{2}$$

Where P is an empirically determined coefficient which increases with increasing surface roughness and atmospheric stability (Huang, 1979). In this study, P is defined 0.15, 0.25 and 0.55 for the atmospheric condition of unstable (A), neutrals (D) and stable (F), respectively. In addition, U^* is the velocity at reference height $z^*(U^* = 3$ m/s), k_v is von Karman's constant (0.41) and Z_* is the surface roughness length in the vertical direction (Z), defined as 7 m, a typical average value for a non-urban area.

2. 3 Treatment of Numerical

The simulations were performed using an implicit in-house CFD code-*FVsolver* (Barzegar Gerdroodbary *et al*., 2016, 2015a-d, 2014, 2012, 2011, 2010; Amini *et al*., 2015). This code solves the Navier-Stokes equations using cell centered finite volume approach. A second order upwind scheme was used to discretize RANS equation and the species transport equation with a SIMPLE algorithm. Four types of equations are solved in each case: the continuity equation (3), RANS equations (4), and two turbulence closure equations (6)- (7) for realizable k-ε, for the turbulent kinetic energy (k), and for the dissipation rate of turbulent kinetic energy (ε). Tauseef *et al*. (2011) showed that the realizable k-ε model is seen to provide more realistic results for heavy gas dispersion in the presence of obstacles, compared to the standard k-ε model, both in time and space.

The continuity equation of incompressible fluid and the Reynolds-averaged Navier-Stokes (RANS) equations are written as follows:

$$\frac{\partial u_i}{\partial x_i} = 0 \tag{3}$$

$$\frac{\partial u_i}{\partial t} + u_j\frac{\partial u_i}{\partial x_j} = -\frac{1}{\rho}\frac{\partial P}{\partial x_i} + \frac{\mu}{\rho}\frac{\partial^2 u_i}{\partial x_j \partial x_j} - \frac{\partial}{\partial x_j}(\overline{u_i' u_j'}) + g_z \tag{4}$$

where, u_j is the jth component of velocity, t is the time, x_j is the jth coordinate, ρ is the density, μ is the dynamic viscosity, and g is the gravitational body force which is in the vertical direction.

$$\overline{u_i' u_j'} = \frac{1}{\rho}\mu_t\left(\frac{\partial u_i}{\partial x_j} + \frac{\partial u_j}{\partial x_i}\right) - \frac{2}{3}k\delta_{ij} \tag{5}$$

Equation (5) is the Reynolds stress equation, where, $\mu_t = \rho C_\mu \frac{k^2}{\varepsilon}$ is the turbulent viscosity. The governing equations of the realizable k-ε turbulence model are

$$\rho\frac{\partial k}{\partial t} + \rho\overline{u}_j\frac{\partial k}{\partial x_j} = \tau_{ij}\frac{\partial \overline{u}_i}{\partial x_j} - \rho\varepsilon + \frac{\partial}{\partial x_j}\left[\left(\mu + \frac{\mu_t}{\sigma_k}\right)\frac{\partial k}{\partial x_j}\right] \tag{6}$$

$$\rho\frac{\partial \varepsilon}{\partial t} + \rho\overline{u}_j\frac{\partial \varepsilon}{\partial x_j} = C_{\varepsilon 1}\frac{\varepsilon}{k}\tau_{ij}\frac{\partial \overline{u}_i}{\partial x_j} - C_{\varepsilon 2}\rho\frac{\varepsilon^2}{k} + \frac{\partial}{\partial x_j}\left[\left(\mu + \frac{\mu_t}{\sigma_\varepsilon}\right)\frac{\partial \varepsilon}{\partial x_j}\right] \tag{7}$$

Where, $\tau_{ij} = 2\mu_t S_{ij} - \frac{2}{3}\rho k\delta_{ij}$ and $S_{ij} = \left(\frac{\partial \overline{u}_i}{\partial x_j} + \frac{\partial \overline{u}_j}{\partial x_i}\right)$. The model constants are $C_\mu = 0.09$, $\sigma_k = 1$, $\sigma_\varepsilon = 1.3$, $C_{\varepsilon 1} = 1.44$ and $C_{\varepsilon 2} = 1.92$ (Tauseef *et al*., 2011; Sini *et al*., 1996). The pollutant dispersion patterns were analyzed, after solving the species transport equation, in conjunction with the turbulence model equations. The advection-diffusion (AD) module was applied to study the species transport process, by analyzing the mass fraction of pollutants in the mixture.

The code analyzes the mass diffusion process based on the species transport equation:

$$\vec{\nabla}\cdot(\rho\vec{V}Y_i) = -\vec{\nabla}\cdot\vec{J_j} \tag{8}$$

$$\vec{J_j} = -\left(\rho D_{i,m} + \frac{\mu_t}{Sc_t}\right)\vec{\nabla}Y_i \tag{9}$$

Where, J_j is the diffusion flux of the mixture (kg/m^{2}s), ρ is the density of the mixture (kg/m^3), $D_{i,m}$ is the mass diffusion coefficient of the pollutant in the mixture (m^2/s), Y_i is the mass fraction of the pollutant (kg/kg), and μ_t is the turbulent viscosity (kg·s/m). Similar to the other studies (Di Sabatino *et al*., 2008; Riddle *et al*., 2004), the turbulent Schmidt number was Sc_t specified as 0.7.

In order to increase convergence, the freestream without ammonia leak was solved as a first step. After the flow field in the vicinity of the barrier is formed, the pollution (NH_3) is issued through a single leak hole. When the jet is released from the leakage, it severely oscillates. After a few iterations, the oscillations are limited and the pollution flow approximately forms a steady flowfield, though some small fluctuations remain. This issue will be completely discussed in the following sections.

3. RESULTS AND DISCUSSION

3.1 Validation

In numerical simulations, the validation of the data is essential for the evaluation of the results. In this paper, the numerical results of NH_3 free dispersion along the downstream surface of the leak are compared with other experimental results to validate the precision of the present study.

To validate the numerical accuracy and obtain a better understanding of fundamental wind-buoyancy-driven flow, the three-dimensional computational domain used in this study is kept identical with the experimental model proposed by Bouet *et al.* (2005), which consists of 3 cases with the different atmospheric conditions and leak rates. The height H of the barrier is 3 m. In addition, the distance of the barrier to leak position is 1 m and 3 m for the second and third tests. The height of the computational domain is kept at 4H. Three experimental tests of Bouet *et al.* (2005) are chosen with/without solid barrier arrangement to compare the dispersion of the ammonia in downstream of leakage (Table 1). Fig. 3 compares the numerical result of the present study and the experimental data of Bouet *et al.* (2005). The experimental data are obtained from a ground-level line-source of ammonia leak. Since the real distribution of gas in the experimental study is in three directions (streamwise, spanwise and vertical directions), the three dimensional domain with 2700000 grids is chosen for the validation. The results in Fig. 3 show good agreement between the simulations and other correlation in models with/without a solid barrier. Furthermore, the comparison verifies that the two dimensional results of the numerical simulation present a small discrepancy from experimental data.

Table 1. Dispersion condition of experimental data.

Model	Free stream condition	Barrier height (m)	Barrier distance to leak (m)	Mass flow rate of leak (Kg/s)
1	D	No	–	0.65
2	A	3	3	4.2
3	D	3	1	4.2

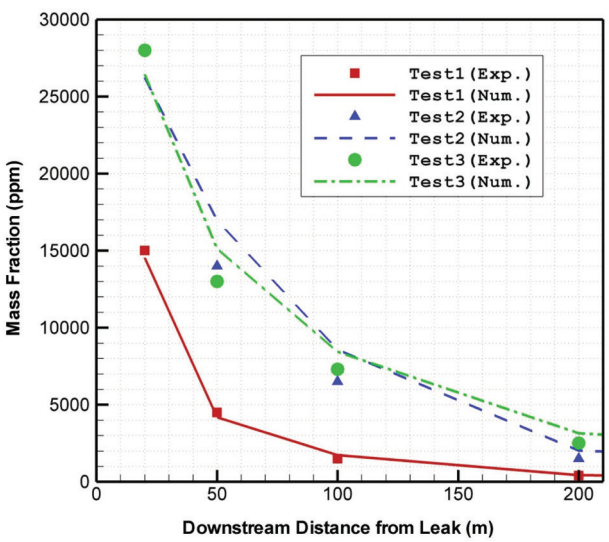

Fig. 3. Mass fraction of Ammonia on ground surface along the symmetry direction (validation).

3.2 Flow Feature of Ammonia Dispersion under Various Mesh Barriers

First, it is expected that the size of the mesh barrier play a significant role in the performance of this device. Therefore, various mesh barriers are examined to evaluate the efficiency of each formation on dispersion. Table 2 shows various arbitrary configurations of the mesh barrier with different Mesh Coefficients.

Fig. 4 compares the influence of different mesh barriers on the dispersion of the ammonia leak (mass flow = 0.2 Kg/s) within a stable atmospheric condition (F). The color region in figures depicts the danger zone where the mass fraction of ammonia is more than 500 ppm. The results illustrate that danger zones extensively varied in the downstream as different mesh barriers are presented. In the case of no barrier, the general features of the ammonia dispersion are typical leakage, such as that presented by previously published works (Bouet *et al.*, 2005). The distribution of the NH_3 clearly shows that the danger zone expands as the ammonia moves to downstream. Since several studies (Schulte *et al.*, 2014; Sklavounos *et al.*, 2014; Steffens *et al.*, 2013, 2012; Dandrieux *et al.*, 2001; Khan *et al.*, 1999a, b) have extensively described about the flow structure of the leak without a barrier, the discussion in this area is referred to these works. However, the presence of low coefficient mesh barrier (case 1 and case 2) leads to the reflection of the free stream immediately downstream

Table 2. Mesh size of barriers in present simulation.

Case	Num. of hole	Hole size (cm)	Barrier distance to leak (m)	Mesh coeff.
1	5	10	3	0.5
2	10	10	3	2
3	10	30	3	6
4	10	40	3	8
5	20	15	3	12
6	20	20	3	16
7	20	15	1.5	12
8	20	15	4.5	12

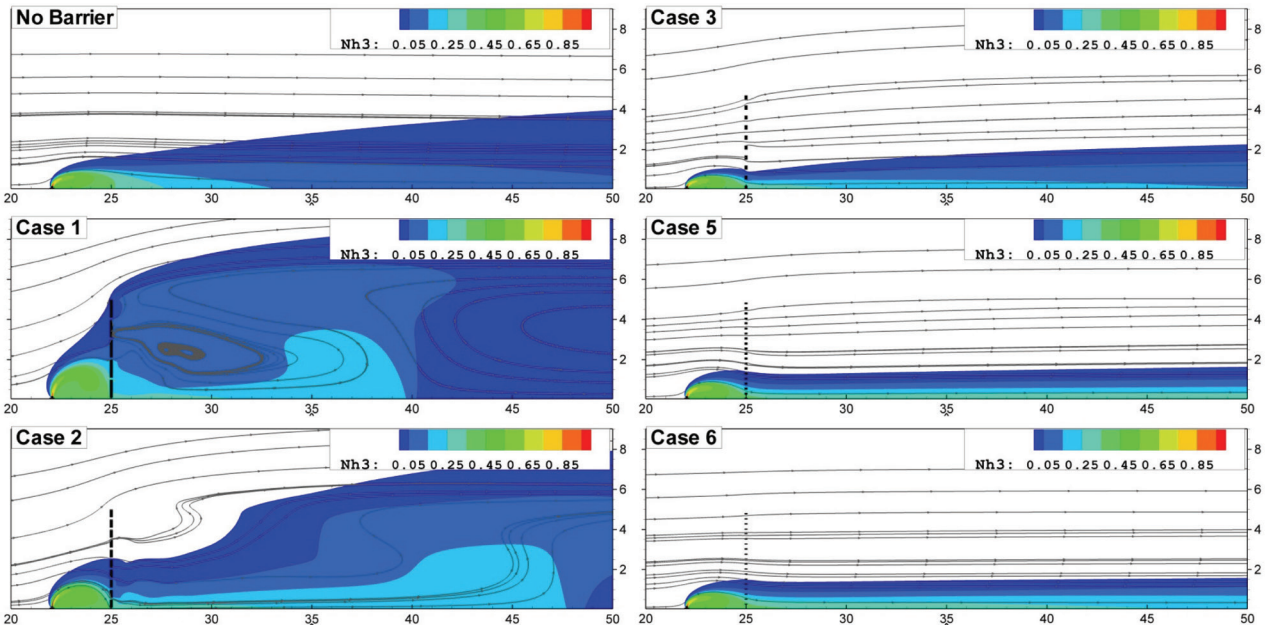

Fig. 4. Influence of various mesh barriers on flow structure and mass concentration of Ammonia leak (Atmospheric condition = F, m° = 0.2 Kg/s). All dimension is in meter.

of the mesh barrier and the stream patterns form similar distribution as they interact with a solid barrier. Then, the danger zone is not only limited but also increased, and the height of the dispersion becomes larger. As the mesh coefficient of the barrier increases, the adverse pressure gradient caused by the solid barrier vanishes and the ammonia disperses at limiting height downstream. In other words, a high amount of the ammonia leak diffuses through the holes of the mesh barrier, and the danger zone is thereby significantly declined.

The height of the danger zone is a crucial factor for the safety and design of the industrial plant where the risk of the leakage is presented. Therefore, extensive efforts were performed to know the risk region. Fig. 5 illustrates the variation of the height of the danger zone along the streamwise direction for various causes in the stable atmospheric condition (F) with low leak rate (mass flow = 0.2 Kg/s). The results clearly show that the danger zone is diminished as a mesh barrier with high Mesh Coefficient are presented in downstream of the leak. In addition, the height of the danger zone significantly reduces when the mesh coefficient is increased. Also, the performance of the mesh on the dispersion is approximately the same in cases with high mesh coefficient (MC = 12 and 16). Thus, incase 5, MC = 12 is chosen as an optimum choice for comparisons of this device in different conditions.

Since the efficiency of this method is significantly high in low leak rate, the careful study of this device

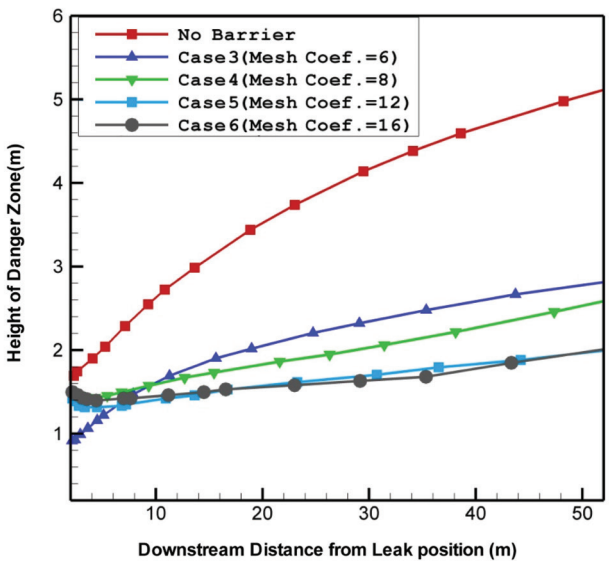

Fig. 5. Comparison of the height of danger zone along the streamwise direction.

will improve our insight and reduce the risk of danger in industrial plants. As the flow pattern due to interaction with a mesh barrier highly influences the dispersion of leaking gas, precise inspection of the flow offers valuable information about the dispersion; and therefore the performance of this device is fully revealed.

Fig. 6 compares three main flow parameters (mass

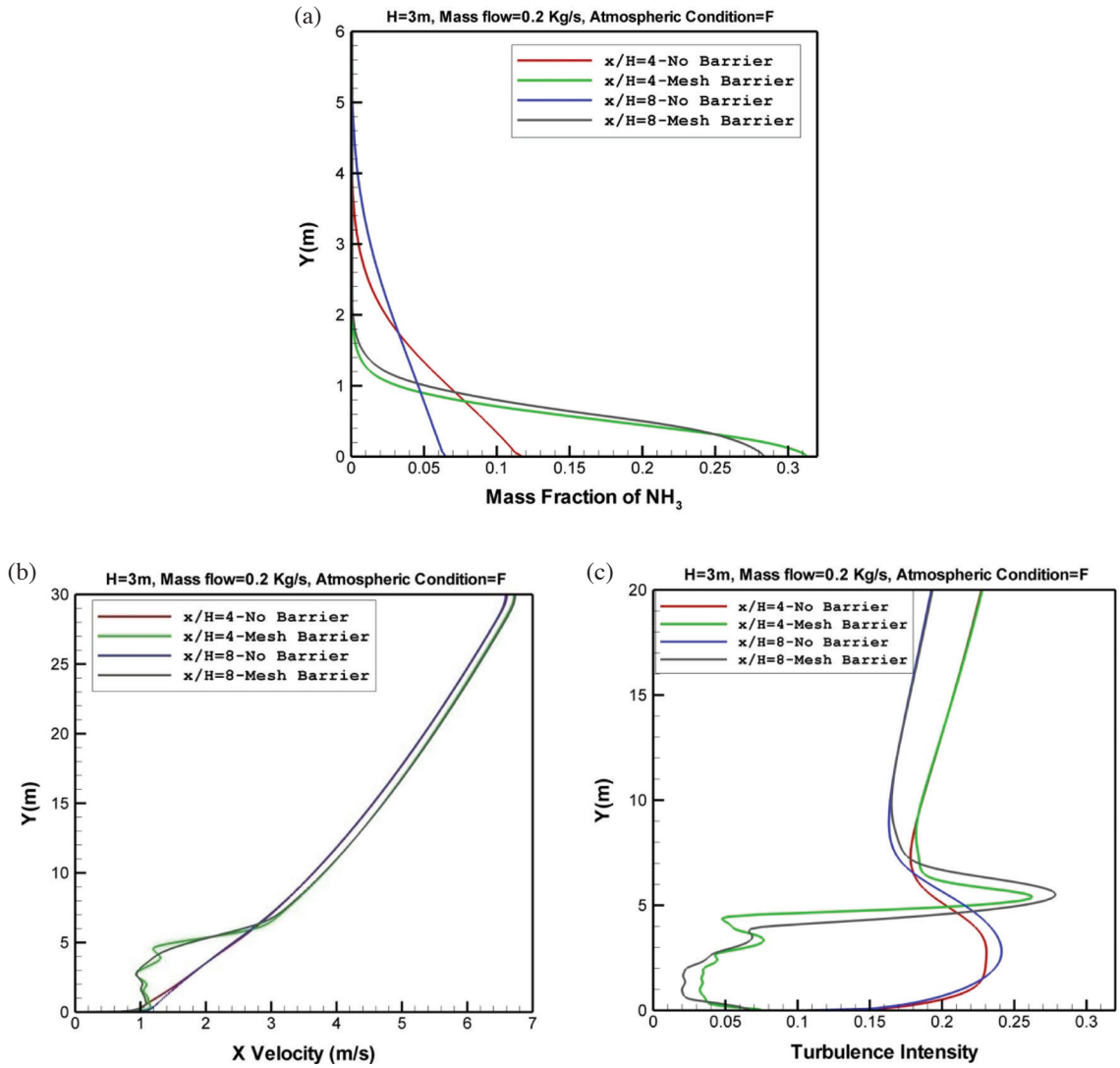

Fig. 6. Comparison of (a) Mass fraction (b) streamwise velocity (c) turbulence intensity with/without mesh barrier with MC = 12 (case 5) on two surfaces (x/H = 4 and x/H = 8) downstream of the leakage (m° = 0.2 Kg/s, Atmospheric condition = F).

fraction, streamwise velocity and turbulence intensity) to investigate the effects of mesh barrier (case 5) on the dispersion of the ammonia. Fig. 6a illustrates the mass concentration profile of the ammonia leak with/without mesh barrier in two distances (x/H = 4 and x/H = 8) from the leakage. The plot depicts that the high volume of the ammonia is directed to ground surface in downstream under the influence of the mesh barrier. Furthermore, the presence of mesh barrier significantly reduces the variation of ammonia mass concentration along the downstream in comparison of no barrier. Therefore, it can be easily detected and collected in the downstream.

The momentum of free stream is highly affected by the presence of the barrier. Fig. 6b clearly shows that the streamwise velocity is reduced (height of the mesh barrier is 5 m) when the mesh barrier is presented in downstream. In fact, uniform flow forms as a free stream passes the mesh barrier and new boundary layer is created.

Turbulence intensity is a main parameter that clearly shows the status (laminar or turbulence) of the free stream pattern. The variation of turbulence intensity is plotted for two distances from the leak in Fig. 6c. The turbulence intensity is defined as the ratio of the root-mean-square of the velocity fluctuations, u′, to the mean flow velocity, u_{ave}. A turbulence intensity of 1% or less is generally considered low and turbulence intensities greater than 10% are considered high. The comparison of the turbulence intensity downstream of the mesh bar-

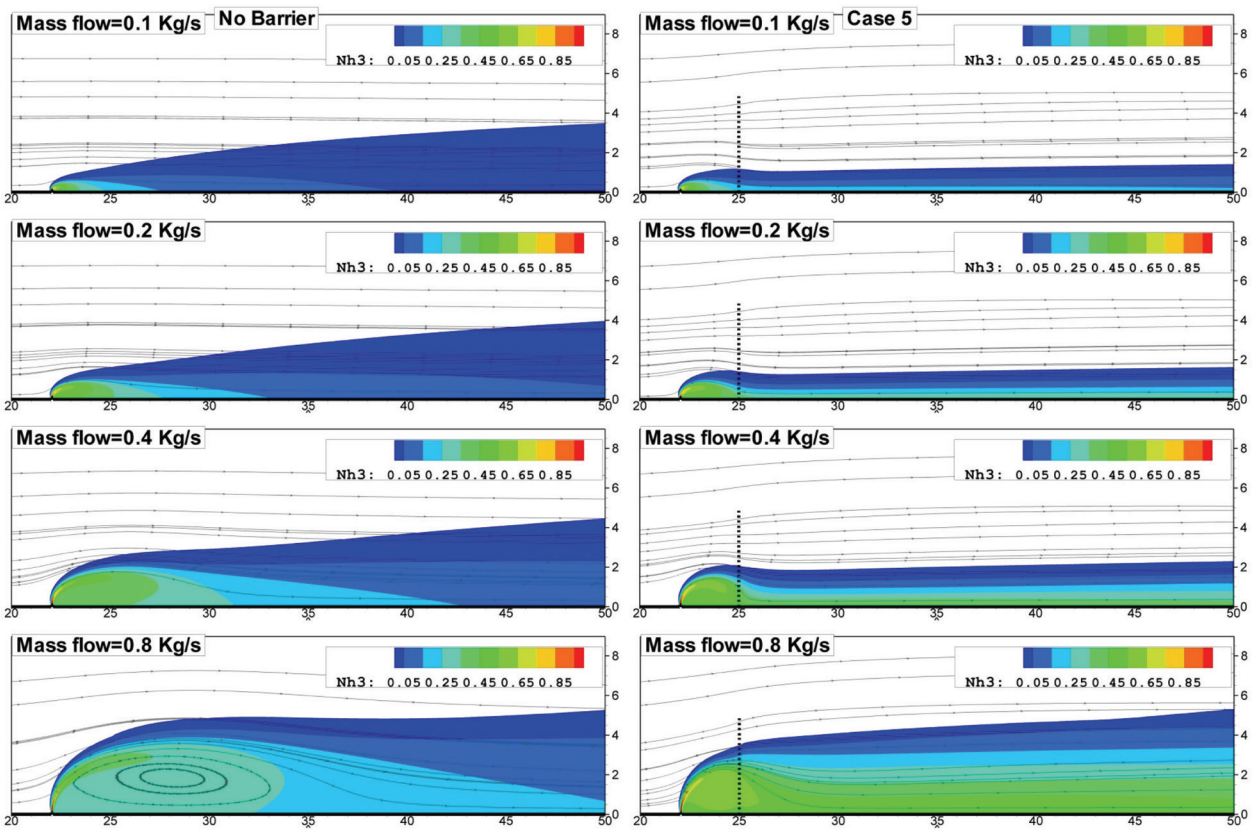

Fig. 7. Comparison of Ammonia dispersion with/without mesh barrier with MC = 12 (case 5) for various leak rates (Atmospheric condition = F). All dimension is in meter.

rier and no barrier clearly shows that the turbulent flow is significantly reduced and flow behaves as laminar in low level. This variation confirms that this device performs as a flow reducer to control the dispersion of gases downstream.

3. 3 Effects of Leak

The mass flow rate and direction of ammonia leak is expected to have a great influence on the performance of the mesh barrier especially on the height of the danger zone. In this section, those changes in structure of dispersion are investigated for four mass flow rates (0.1, 0.2, 0.4 and 0.8 Kg/s) and three leak directions (co-flow, cross flow and counter-flow). To illustrate the effects of mass flow rate, Fig. 7 comparesmass concentration contours along the leak centerline with streamline patterns for a stable atmospheric condition (F). As expected, the danger zone is expanded as the leak rate is increased. Furthermore, the influence of the mesh barrier is more visible in the limitation of ammonia dispersion in the low flow rate (equal or less than 0.4 Kg/s). As expected, the size of danger zone does not change when the leak rate is high. In fact, this method cannot limit the height of the danger zone, and the mesh barrier with high mesh coefficient (12) performs in the same way as free dispersion (no barrier). However, the profile of the ammonia mass fraction is similar in the vertical direction for all leak rates.

Fig. 8 illustrates the dispersion of NH_3 leak with three directions (co-flow, cross flow and counter-flow) in the presence of a mesh barrier (case 5) for a small leak rate ($m^o = 0.2$ Kg) under stable atmospheric condition (F). The result shows a significant structure to the danger zone downstream of the leak. In cases of no barrier, the leak distribution is approximately the same domain although the slope of boundary of danger zone is different. On the other hand, the expansion of danger zone is significantly reduced within specific level when the mesh barrier is presented downstream of the leak. In all cases with a mesh barrier, the height of the danger zone is fixed at the same level that a leak gas passes the barrier.

3. 4 Atmospheric Condition

Fig. 9 depicts the influence of the mesh barrier (case 5) on the distribution of ammonia ($m^o = 0.2$ Kg/s) in

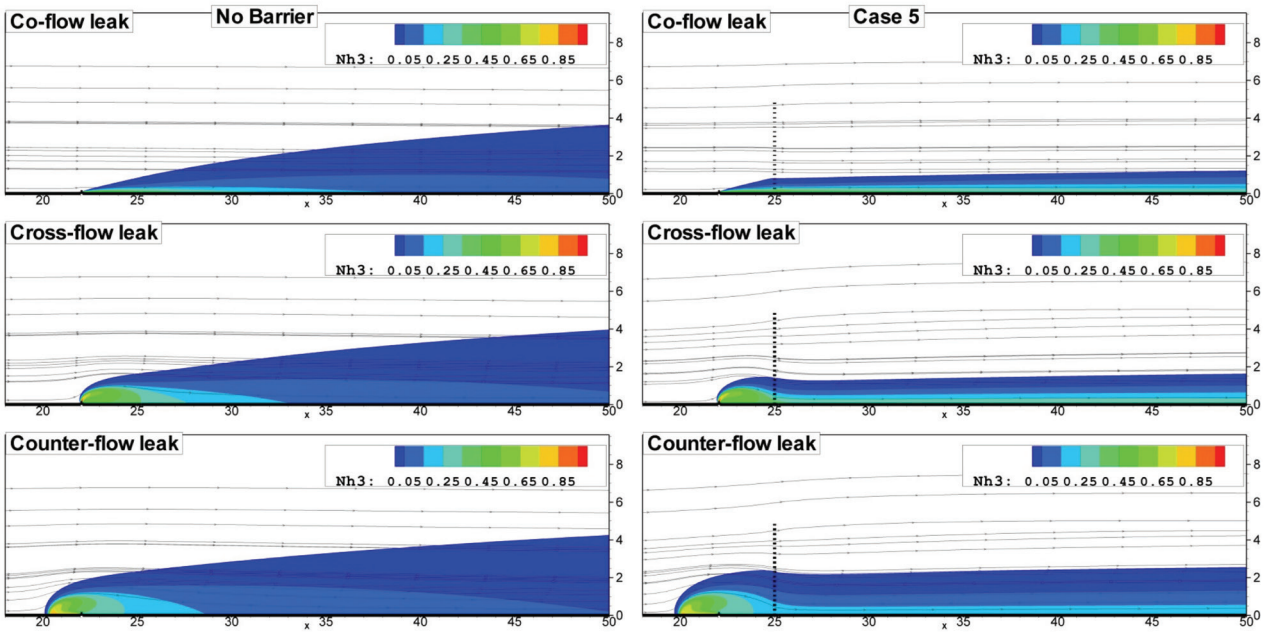

Fig. 8. Influence of leak direction on dispersion with/without mesh barrier with MC = 12 (case 5) (Atmospheric condition = F, $\dot{m}$ = 0.2 Kg/s). All dimension is in meter.

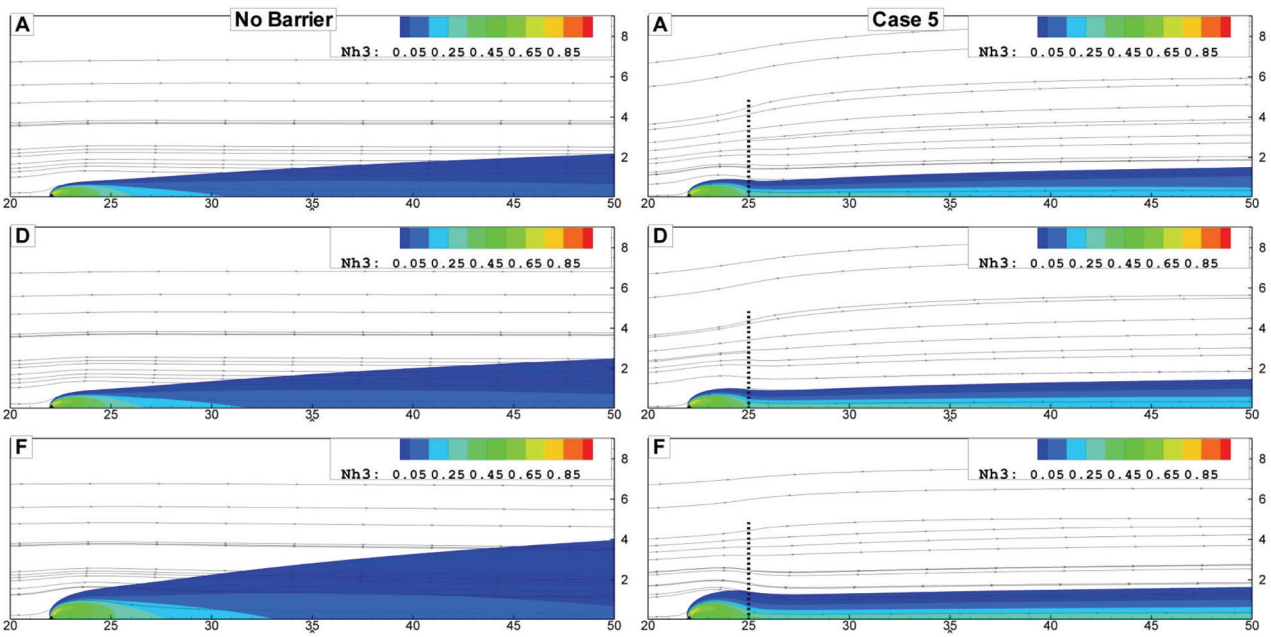

Fig. 9. Comparison of atmospheric condition on size of danger zone with/without mesh barrier with MC = 12 (case 5) ($\dot{m}$ = 0.2 Kg/s). All dimension is in meter.

three atmospheric conditions (unstable, neutral and stable). In order to present a different atmospheric conditions, inlet velocity profiles are varied corresponds to atmospheric stability conditions. As expected, the danger zone highly expands under the stable atmospheric condition (F) in free dispersion. As a mesh barrier is presented in the downstream of the leak, the height of the toxic region is reduced. The maximum concentra-

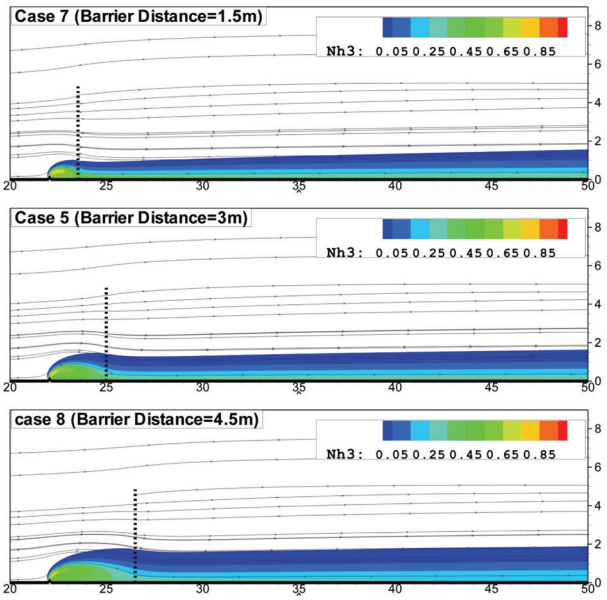

Fig. 10. The influence of the mesh barrier distance on dispersion of Ammonia (Atmospheric condition = F, m° = 0.2 Kg/s). All dimension is in meter.

tion of ammonia is at the vicinity of the leak in the free dispersion. As the mesh barrier is presented in the domain, the maximum ammonia concentration is occurred in the ground surface along the domain. In fact, the mesh barrier performs in the same way in various conditions and the height of the danger zone is limited.

3. 5 Distance Barrier

Fig. 10 exhibits the mass dispersion of ammonia leak in the presence of the mesh barrier with three different distances (1.5, 3 and 4.5 m) from the leak position. As the barrier moves downstream, the penetration of ammonia increases in the vertical direction and the height of the danger zone is extended in the streamwise direction. The mesh barrier fixes the height of dispersion as the gas emitted from holes. The performance of the device increases significantly as it moves to the leak position.

4. CONCLUSION

Numerical simulations have been performed to investigate the effect of using a mesh barrier on the dispersion of ammonia as a leak from a pipeline in a various atmospheric conditions. Parameters such as leak rates, leak direction and barrier mesh size have been studied to cover all aspects of the flow behavior of the mesh barrier in free streams on a flat surface. The results allow us to present the following conclusions:

1) In all cases with high mesh coefficient (MC), the presence of a mesh barrier substantially limits on the dispersion of ammonia in downstream for various atmospheric conditions. In addition, the height of the toxic zone in downstream from leak exhibits a wide range of variations related to the leak rate and the mesh size of the barrier. The mass distribution of the ammonia leak in the presence of a mesh barrier is very different from free dispersion. According to obtained data in various atmospheric conditions, a mesh barrier with MC = 12 is recommended to mitigate the danger zone in the vicinity of the toxic leak in all conditions.
2) Variations in the leak rate have a strong effect on the performance of the mesh barrier on flow behavior and dispersion. At low mass flow rates, the dispersion is small and a mesh barrier easily restricts the danger zone. As the mass flow rate of leak is increased, the effect of mesh barrier on distribution decreases. The results show that the performance of the mesh barrier on the dispersion is optimal when the leak flow rate is equal to, or less than 0.4 kg/s.
3) In mesh barrier cases, variations in barrier distance from the leak also play a significant role in the performance and dispersion of gases such as ammonia downstream. At very close spacing, weak interaction is observed and leak penetration is limited. Therefore, the performance of the mesh barrier is substantial. As the spacing is increased, the larger spatial freedom allows the leak to develop more naturally, leading to a large dispersion zone under the influence of the free stream velocity. Subsequently, leak mixing is highly increased and the toxic zone is expanded downstream. Hence, a mesh barrier limited the height of the danger zone to a higher level than in the case of a close space.

REFERENCES

Amini, Y., Mokhtari, M., Haghshenasfard, M., Gerdroodbary, M.B. (2015) Heat transfer of swirling impinging jets ejected from Nozzles with twisted tapes utilizing CFD technique, Case Studies in Thermal Engineering 6, 104-115.

Barzegar Gerdroodbary, M., Bishesari, Sh., Hosseinalipour, S.M., Sedighi, K. (2012) Transient Analysis of Counterflowing Jet over Highly Blunt Cone in Hypersonic Flow. Acta Astronautica 73, 38-48.

Barzegar Gerdroodbary, M., Fayazbakhsh, M.A. (2011) Numerical Study on Heat Reduction of Various Counterflowing Jets over Highly Blunt Cone in Hypersonic.

International Journal of Hypersonics 2, 1-13.
Barzegar Gerdroodbary, M., Ganji, D.D., Amini, Y. (2015) Numerical study of shock wave interaction on transverse jets through multiport injector arrays in supersonic crossflow. Acta Astronautica 115, 422-433.
Barzegar Gerdroodbary, M., Hosseinalipour, S.M. (2010) Numerical simulation of hypersonic flow over highly blunted cones with spike. Acta Astronautica 67, 180-193.
Barzegar Gerdroodbary, M., Imani, M., Ganji, D.D. (2014) Heat reduction using conterflowing jet for a nose cone with Aerodisk in hypersonic Flow. Aerospaces Sciences and Technology 39, 652-665.
Barzegar Gerdroodbary, M., Imani, M., Ganji, D.D. (2015) Investigation of film cooling on nose cone by a forward facing array of micro-jets in Hypersonic Flow. International Communications in Heat and Mass Transfer 64, 42-49.
Barzegar Gerdroodbary, M., Jahanian, O., Mokhtari, M. (2015) Influence of the Angle of Incident Shock Wave on Mixing of Transverse Hydrogen Micro-jets in Supersonic Crossflow. International Journal of Hydrogen Energy 40, 9590-9601.
Barzegar Gerdroodbary, M., Rahimi Takami, M., Ganji, D.D. (2015) Investigation of thermal radiation on traditional Jeffery-Hamel flow to stretchable convergent/divergent channels. Case Studies Thermal Engineering 6, 28-39.
Barzegar Gerdroodbary, M., Takami, M.R., Heidari, H.R., Fallah, K., Ganji, D.D. (2016) Comparison of the single/multi Transverse jets under the influence of shock wave in Supersonic Crossflow. Acta Astronautica 123, 283-291.
Bouet, R., Duplantier, S., Salvi, O. (2005) Ammonia large scale atmospheric dispersion experiments in industrial configurations. Journal of Loss Prevention in the Process Industries 18, 512-519.
Bubbico, R., Mazzarotta, B., Verdone, N. (2014) CFD analysis of the dispersion of toxic materials in road tunnels. Journal of Loss Prevention in the Process Industries 28, 47-59.
Cheng, Ch., Tan, W., Liu, L. (2014) Numerical simulation of water curtain application for ammonia release dispersion. Journal of Loss Prevention in the process Industries 30, 105-112.
Dandrieux, A., Dusserre, G., Ollivier, J., Fournet, H. (2001) Effectiveness of water curtains to protect firemen in case of an accidental release of ammonia: comparison of the effectiveness for two different release rates of ammonia. Journal of Loss Prevention in the Process Industries 14, 349-355.
Di Sabatino, S., Buccolieri, R., Pulvirenti, B., Britter, R. (2008) Flow and pollutant dispersion in street canyons using FLUENT and ADMS-Urban. Environmental Modeling and Assessment 13, 369-381.
Galeev, A.D., Ponikarov, S.I. (2014) Numerical analysis of toxic cloud generation and dispersion: A case study of the ethylene oxide spill. Process Safety and Environmental Protection 92, 702-713.
Galeev, A.D., Starovoytova, E.V., Ponikarov, S.I. (2013a) Numerical simulation of the consequences of liquefied ammonia instantaneous release using FLUENT software. Process Safety and Environmental Protection 91, 191-201.
Galeev, A.D., Salin, A.A., Ponikarov, S.I. (2013b) Consequence analysis of aqueous ammonia spill using computational fluid dynamics. Journal of Loss Prevention in the Process Industries 26, 628-638.
Huang, C.H. (1979) Theory of dispersion in turbulent shear flow. Atmospheric Environment 13, 453-463.
Jeong, S.J. (2014) Effect of Double Noise-Barrier on Air Pollution Dispersion around Road, Using CFD. Asian Journal of Atmospheric Environment 8(2), 81-88.
Khan, F.I., Abbasi, S.A. (1999a) Modelling and control of the dispersion of hazardous heavy gases. Journal of Loss Prevention in the Process Industries 12, 235-244.
Khan, F.I., Abbasi, S.A. (1999b) HAZDIG: a new software package for assessing the risks of accidental release of toxic chemicals. Journal of Loss Prevention in the Process Industries 12, 167-181.
Khan, F.I., Abbasi, S.A. (2000) Cushioning the impact of toxic release from runaway industrial accidents with greenbelts. Journal of Loss Prevention in the Process Industries 13, 109-124.
Labovský, J., Jelemenský, L′. (2011) Verification of CFD pollution dispersion modelling based on experimental data. Journal of Loss Prevention in the Process Industries 24, 166-177.
Mack, A., Spruijt, M.P.N. (2013) Validation of OpenFoam for heavy gas dispersion applications. Journal of Hazardous Materials 262, 504-516.
Ng, W.Y., Chau, C.K. (2014) A modeling investigation of the impact of street and building configurations on personal air pollutant exposure in isolated deep urban canyons. Science of the Total Environment 468-469.
Pandya, N., Gabas, N., Marsden, E. (2012) Sensitivity analysis of Phast's atmospheric dispersion model for three toxic materials (nitric oxide, ammonia, chlorine). Journal of Loss Prevention in the Process Industries 25, 20-32.
Pasquill, F. (1961) The estimation of the dispersion of windborne material. The Meteorological Magazine 90(1063), 33-49.
Riddle, A., Carruthers, D., Sharpe, A., McHugh, C., Stocker, J. (2004) Comparison between FLUENT and ADMS for atmospheric dispersion modeling. Atmospheric Environment 38, 1029-1038.
Schulte, N., Snyder, M., Isakov, V., Heist, D., Venkatram, A. (2014) Effects of solid barriers on dispersion of roadway emissions. Atmospheric Environment 97, 286-295.
Sini, J.F., Anquetin, S., Mestayer, P.G. (1996) Pollutant dispersion and thermal effects in urban street canyons. Atmospheric Environment 30, 2659-2677.
Sklavounos, S., Rigas, F. (2004) Validation of turbulence models in heavy gas dispersion over obstacles. Journal of Hazardous Materials 108, 9-20.

Steffens, J.T., Heist, D.K., Perry, S.G., Zhang, K.M. (2013) Modeling the effects of a solid barrier on pollutant dispersion under various atmospheric stability conditions. Atmospheric Environment 69, 76-85.

Steffens, J.T., Wang, Y.J., Zhang, K.M. (2012) Exploration of effects of a vegetation barrier on particle size distributions in a near-road environment. Atmospheric Environment 50, 120-128.

Tauseef, S.M., Rashtchian, D., Abbasi, S.A. (2011) CFD-based simulation of dense gas dispersion in presence of obstacles. Journal of Loss Prevention in the Process Industries 24, 371-376.

Vallero, D., Isukapalli, S. (2014) Simulating real-world exposures during emergency events: Studying effects of indoor and outdoor releases in the Urban Dispersion Program In upper Manhattan, NewYork. Journal of Exposure Science and Environmental Epidemiology 24, 279-289.

(Received 23 February 2016, revised 24 June 2016, accepted 4 July 2016)